The structure of coxsackievirus B3 at 3.5 Å resolution

Jodi K Muckelbauer[1], Marcia Kremer[1], Iwona Minor[1], Guy Diana[2], Frank J Dutko[3], James Groarke[2], Daniel C Pevear[2] and Michael G Rossmann[1]*

[1]Department of Biological Sciences, Purdue University, 1392 Lilly Hall of Life Science, West Lafayette, IN 47907, USA, [2]ViroPharma, Inc., 1250 S. Collegeville Road, Collegeville, PA 19426, USA and [3]Department of Virology, Sterling Winthrop Pharmaceuticals Research Division, 1250 S. Collegeville Road, Collegeville, PA 19426, USA

Background: Group B coxsackieviruses (CVBs) are etiologic agents of a number of human diseases that range in severity from asymptomatic to lethal infections. They are small, single-stranded RNA icosahedral viruses that belong to the enterovirus genus of the picornavirus family. Structural studies were initiated in light of the information available on the cellular receptors for this virus and to assist in the design of antiviral capsid-binding compounds for the CVBs.

Results: The structure of coxsackievirus B3 (CVB3) has been solved to a resolution of 3.5 Å. The β-sandwich structure of the viral capsid proteins VP1, VP2 and VP3 is conserved between CVB3 and other picornaviruses. Structural differences between CVB3 and other enteroviruses and rhinoviruses are located primarily on the viral surface. The hydrophobic pocket of the VP1 β-sandwich is occupied by a pocket factor, modeled as a C_{16} fatty acid. An additional study has shown that the pocket factor can be displaced by an antiviral compound. Myristate was observed covalently linked to the N terminus of VP4. Density consistent with the presence of ions was observed on the icosahedral threefold and fivefold axes.

Conclusions: The canyon and twofold depression, major surface depressions, are predicted to be the primary and secondary receptor-binding sites on CVB3, respectively. Neutralizing immunogenic sites are predicted to lie on the extreme surfaces of the capsid at sites that lack amino acid sequence conservation among the CVBs. The ions located on the icosahedral threefold and fivefold axes together with the pocket factor may contribute to the pH stability of the coxsackieviruses.

Structure 15 July 1995, **3**:653–667
Key words: coxsackievirus B3, enterovirus, viral myocarditis

Introduction

Picornaviruses are a family of small, non-enveloped, single-stranded positive-sense RNA viruses. The coding region of the RNA genome contains a single open reading frame and is translated into one polypeptide. The structural proteins are cleaved by virally encoded proteinases to yield VP0, VP3 and VP1. Assembly into mature virion particles is completed by the autocatalytic cleavage of VP0 into VP4 and VP2. The mature virions are approximately 300 Å in diameter and the interior of the capsid shell is packed with single-stranded RNA [1]. The virus capsid is composed of 60 protomers, each consisting of one copy of viral proteins VP1–4 arranged in a T=1 (pseudo T=3) icosahedral lattice [2]. Molecular weights for picornaviruses, including the RNA, are on the order of 8×10^6 Da.

In the picornavirus family, the five major genera are the enteroviruses, rhinoviruses, aphthoviruses, cardioviruses and hepatoviruses [1]. They are distinguished by physical properties (pH stability and buoyant density), clinical syndromes [3] and RNA sequence [4]. Atomic resolution structures are available for four of the five major genera [5–8]. The enteroviruses are pH stable and survive passage through the stomach to the lower intestinal tract, where replication takes place. The enteroviruses of humans are further classified, on the basis of clinical manifestations, into polioviruses (3 serotypes), coxsackie A (23 serotypes) and B (6 serotypes) viruses, echoviruses (34 serotypes) and human enteroviruses (5 serotypes) [3].

Cell-surface receptors have been isolated and identified for a number of picornaviruses. Some of the receptors are members of the immunoglobulin superfamily [9–12], whereas others belong to different protein classes [13–16]. The locations of receptor-binding sites for human rhinovirus (HRV)-16 [17] and HRV14 (N Olson, P Kolatkar, M Rossmann and T Baker, unpublished data) have been determined using cryoelectron microscopy and image reconstruction. These studies showed that intercellular adhesion molecule-1 (ICAM-1), the receptor for the major group of rhinoviruses, binds into a 15 Å deep canyon surrounding the icosahedral fivefold axes, and corroborated the canyon hypothesis [18] which was proposed previously based on the three-dimensional structure of HRV14 [5], the conservation of amino acid residues lining the canyon [19,20] and mutational studies of amino acids located inside the canyon of rhinoviruses [21] and polioviruses [22].

There is evidence for two CVB receptors on human HeLa cells: human receptor 1 (HR1) and human receptor 2 (HR2). HR1 is an unidentified 50 kDa protein which is recognized by all six CVB serotypes and is probably the major functional receptor for the CVBs [23]. HR2 [24] is a 60–70 kDa protein, recently identified as

*Corresponding author.

 ISSN 0969-2126

decay-accelerating factor (DAF) or CD55, which is a complement regulatory protein [25]. DAF is also a receptor for a number of echoviruses [15,16]. The HR2 receptor was identified by isolating variants of CVB3 that had been adapted to grow on rhabdomyosarcoma (RD) cells which are normally not susceptible to CVB3 infection [26]. The ability of these variants to grow on RD cells was attributed to altered receptor susceptibility of the virus. HR2, whose function in cell infectivity is not clear, is probably a minor, low-affinity receptor on HeLa cells. The identification of at least two CVB receptors suggests that these viruses may have the ability to recognize and utilize multiple receptors. Alternatively, they may be part of a receptor complex comprising a number of different proteins, including HR1 and HR2, that define the CVB receptor.

Virus-binding competition studies have revealed that some viruses within the picornavirus family share the same receptors with other picornaviruses as well as with unrelated viruses. Coxsackievirus A21 competes directly with HRV14 for its receptor, ICAM-1, and CVB3 competes for receptor with an unrelated virus, adenovirus 2 (Ad2) [27]. The structure of the receptor-binding domain of the fiber protein of adenovirus 5 (Ad5), a virus which is closely related to Ad2, has been solved by X-ray crystallography [28]. Structural analysis of both CVB3 and the Ad5 fiber protein would be expected to reveal similarities in surface topologies and important features involved in virus–receptor interactions.

Sterling Winthrop Pharmaceuticals Research Division (SWPRD) and others [29] have synthesized a number of antiviral agents that are active against rhinoviruses, polioviruses, coxsackieviruses and other enteroviruses by inhibiting viral uncoating [30] and sometimes also by blocking attachment of the virus to the cell [31,32]. Crystallographic studies have shown that these antiviral compounds bind beneath the canyon floor in a hydrophobic pocket within the β-sandwich of VP1 [33–37]. When antiviral compounds bind into the drug-binding pocket of HRV14 they cause large conformational changes, localized to the βH strand and GH loop of VP1, deforming the canyon floor and blocking receptor attachment [31,32]. The native structures of poliovirus 1-Mahoney (PV1/M), poliovirus 3-Sabin (PV3/S), HRV1A and HRV16 revealed that the drug-binding pocket was occupied in its native state by an unidentified cofactor called the pocket factor [36,38,39]. The pocket factor is displaced when the drugs bind and, hence, in the case of HRV1A, HRV16 and polioviruses, the drugs do not cause significant conformational change upon binding. It has been suggested that the pocket factor functions both to stabilize the virion when in transit between cells, and to destabilize the capsid after attachment prior to uncoating [36,37]. Although pocket factors have been modeled as fatty acids, on the basis of the shape of observed electron density and their hydrophobic environments, they have not been chemically identified.

Here we present the 3.5 Å resolution structure of CVB3 together with an analysis of CVB3 in complex with an antiviral WIN compound.

Results and discussion

Quality of the electron-density map

Overall, the quality of the electron-density map at 3.5 Å resolution was very good. The main-chain density was continuous at a density level of 3σ above background (apart from the regions mentioned below). This allowed the CVB3 amino acid sequence to be built into the electron-density map without ambiguity. VP1, VP2 and VP3 have the conserved β-sandwich folding motif observed for many icosahedral viruses (Fig. 1) [40]. The β-sandwich consists of eight antiparallel β-strands, B–I, that form two sheets, BIDG and CHEF.

Regions of the amino acid sequence for which there was no electron density were as follows: in VP1, the N-terminal residues 1001–1012 (amino acid numbering convention adds 1000, 2000, 3000 and 4000 to the residues of VP1, VP2, VP3 and VP4, respectively) and residues 1128 and 1130; in VP2, the N-terminal residues 2001–2008; and in VP4, residues 4012–4024. The two residues Thr1128 and Gln1130, missing from the electron density for VP1, are located on the exterior DE loop surrounding the icosahedral fivefold axis with Cα atoms at a viral radius of 163 Å. The lack of density for these residues results from the electron density averaging procedure, which used a spherical mask that was slightly too small (outer radius of 162 Å). Residues with weak side-chain densities include: Glu1026, Lys1054, Lys1085, Lys1259, Thr1281, Tyr2009, Lys2043, Lys2158, Lys2166, Gln2263, Arg3035, Lys3041, Glu3060, Arg3073, Ser3078, Lys3144, Gln4004, Gln4048 and Asn4069. All of these residues are polar and are located on the exterior or interior surfaces of the virus capsid where they are exposed to solvent.

Structure of VP1

The N-terminal 12 amino acids of VP1 are absent in the CVB3 electron density. However, evidence from poliovirus structures suggests that the N-terminal five amino acids interact with the N terminus of VP4 at the fivefold axis [38]. The electron-density map of CVB3 shows very weak density, resembling β-structure, beneath residues 4001–4008 of VP4 which may, by analogy to the polioviruses, be the N terminus of VP1. The interaction of the N termini of VP1 and VP4 is consistent with the observation that the N terminus of VP1 is externalized and becomes exposed to proteases upon the formation of altered ('A') particles which lack VP4 [41,42].

The DE loop (residues 1125–1137) is the most prominent of the exterior loops found at the fivefold axis. It runs closest and parallel to the fivefold axis and, as a result, makes extensive interactions with its icosahedral fivefold-symmetry-related DE loops. The size and orientation of the CVB3 DE loop presents greater opportunity for these symmetry-related interactions to occur as

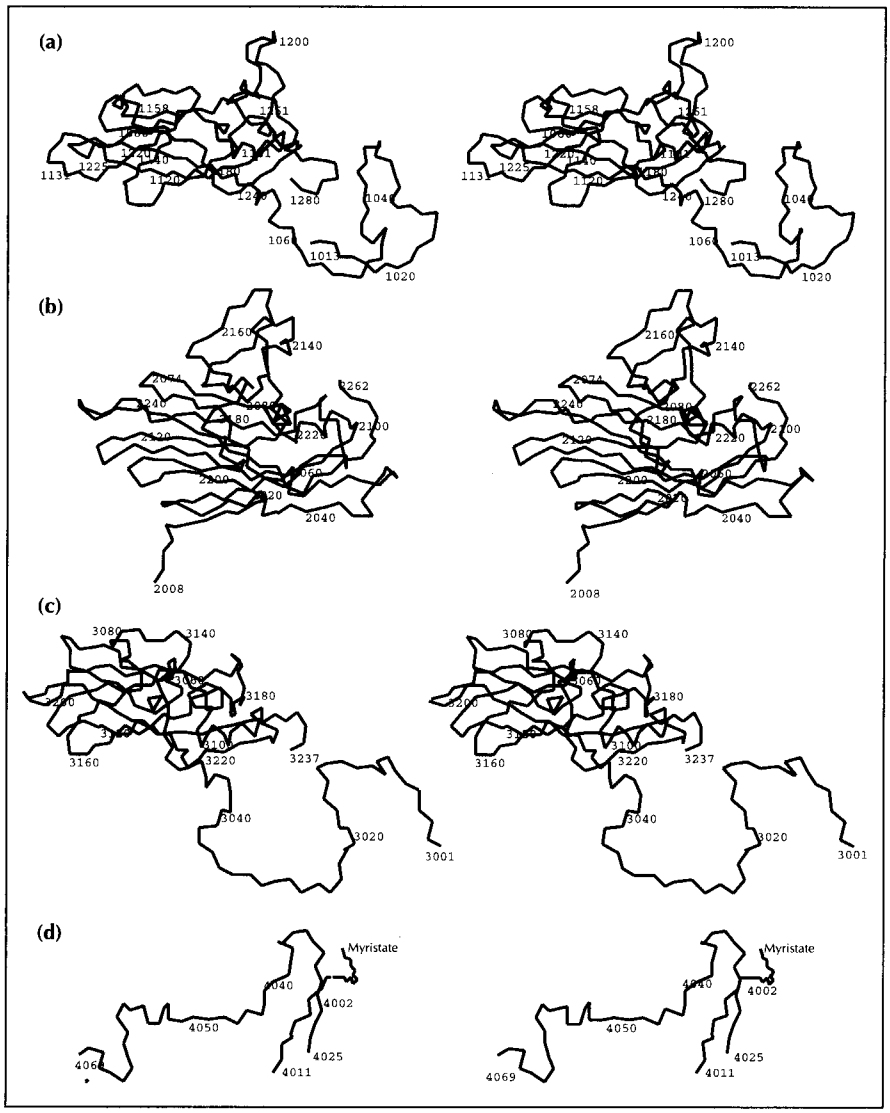

Fig. 1. Stereo Cα traces for **(a)** VP1, **(b)** VP2, **(c)** VP3 and **(d)** VP4 of CVB3 with every 20th residue labeled.

compared with the shorter DE loops of PV1/M and HRV14. Residues in the DE loop are also involved in interactions with putative ion-binding sites (see below) along the fivefold axis. Because of the length and extensive protein–protein and protein–ion interactions, the DE loop may help stabilize virus pentamers and be partially responsible for the pH stability of CVB3. In addition to the stabilizing role of the DE loop, Caggana *et al.* [43] have identified a single amino acid (Thr1129) on the DE loop that is a major determinant of virulence, characterized by pancreatitis and hypoglycemia in mice, for CVB4. Therefore, it appears that the DE loop may play a role in both virion stability and pathogenicity.

The BC loop (residues 1081–1085) is nine (and five) amino acids shorter than the BC loop of HRV14 (and PV1/M) and, as a consequence, it is not as prominent a surface loop as it is for the polioviruses and rhinoviruses. This loop flanks the rim of the canyon closest to the fivefold axes and is an important neutralizing immunogenic (NIm) site for the polioviruses and rhinoviruses [44–47]. CVB4/CVB3 chimera studies have shown that the BC loop of CVB4 contains a major NIm site [48]. Residues located on the BC loop have been shown to be responsible for the host-range specificity of poliovirus 2-Lansing (PV2/L) [49] and, in the case of HRV14 and HRV16, residues in the BC loop are located within the ICAM-1 receptor 'footprint' and may play a role in receptor recognition.

A long, thin, worm-like density feature was found inside the VP1 β-sandwich at the binding site of antiviral compounds (discussed below). The height of the electron density within the pocket was roughly 85–90% of that of the surrounding protein and somewhat weaker at the interior end of the pocket, towards the fivefold axis. This suggested that the pocket in each of the 60 protomers might be fully occupied with a purely carbon compound, that the pocket was not fully occupied or that the moieties in the pocket were not of homogeneous length. The unidentified pocket factor, modeled as a palmitate molecule (16 carbon fatty acid; Fig. 2a), is very similar in size and shape to that observed in PV1/M and PV3/S [38]. The polar head group of the pocket factor is towards the exterior or 'pore' end of the pocket while the aliphatic chain extends the length of the

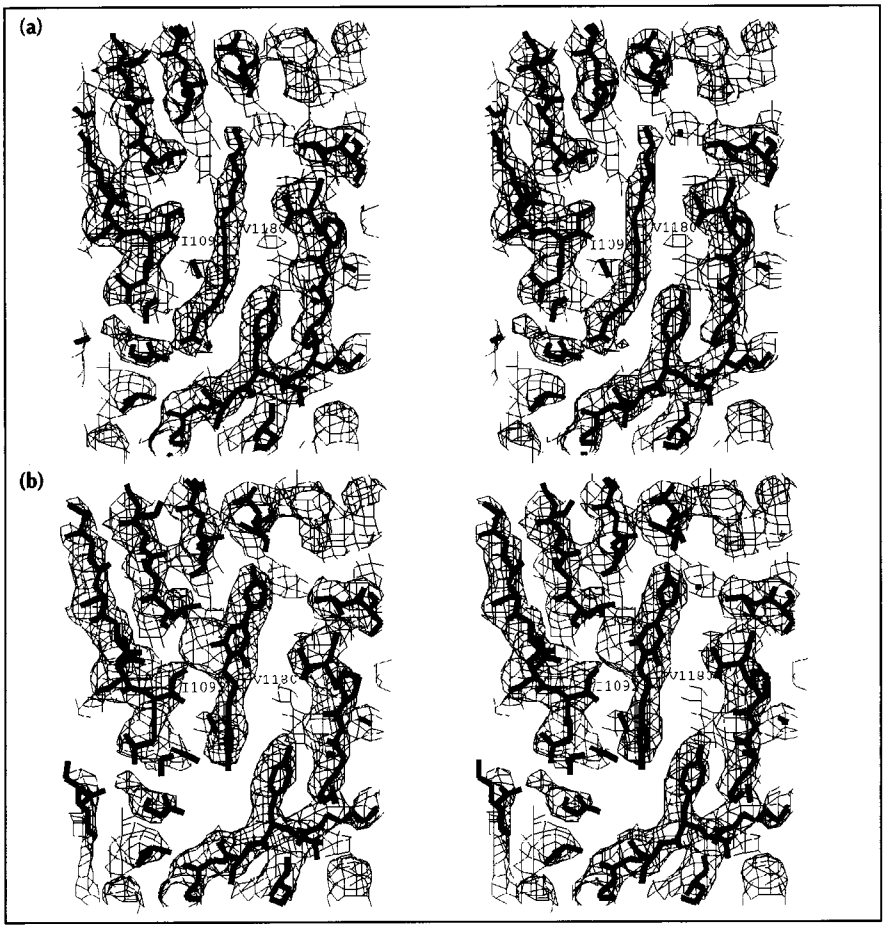

Fig. 2. Averaged electron density maps showing the VP1 β-sandwich pocket. **(a)** CVB3 native electron density and structure showing the pocket factor in the middle of the figure, modeled as palmitate. The map was computed with $|F_{native}|$ (unit weights) coefficients and the final phases determined by molecular replacement electron density averaging. The model is that obtained from X-PLOR refinement. The structure of the palmitate molecule, representing the pocket factor, was obtained by graphical model building. **(b)** CVB3 in complex with the antiviral compound WIN 66393 (see Table 1). The view is the same as shown for (a). The iodine atom can be seen as a prominent area of density adjacent to the phenyl ring of the drug. The map was computed with $(|F_{win}|-k|F_{native}|)$(unit weights) coefficients where k=0.65 was chosen to equalize the density for the WIN compound and the protein. The superimposed structure is as in (a). The WIN compound structure is based on graphical model building. $|F_{native}|$ and $|F_{win}|$ are the structure amplitudes for the native and drug-soaked crystals.

hydrophobic pocket towards the fivefold axis. For the two oxygens of the polar head group, the electron density suggests that one oxygen forms a hydrogen bond with the side-chain nitrogen of Arg1095 while the second oxygen may interact indirectly with the side-chain oxygen of Ser1184 via a water molecule. The carbon chain of the fatty acid makes extensive interactions with the side chains of hydrophobic residues lining the β-sandwich pocket (Table 1). When comparing the position of the pocket factors for CVB3, PV1/M, HRV1A and HRV16, the polar head groups are all in similar locations at the pore end of the pocket whereas the aliphatic chains differ significantly in their conformations and lengths with respect to each other (Fig. 3). Presumably, this reflects the different shapes of the pocket interiors for each of the viruses, which are defined by the amino acids that line the pocket.

Structure of VP2

It has been suggested that the conserved residue Ser2010 is involved in the autocatalytic cleavage of VP0 to VP4 and VP2 [50]. However, mutational analysis has shown that this residue is not essential for the rhinoviruses and polioviruses [51,52]. For CVB3, a hydrogen bond exists between Asp2011 and Asn4069, suggesting an autocatalytic cleavage mechanism that utilizes an aspartate residue similar to that proposed for the nodaviruses [53]. The recent structure of PV1/M [54], in which VP0 has not been cleaved, shows that the region near the C terminus of VP4 and the N terminus of VP2 is very different in the cleaved and uncleaved structures. Prior to the maturation cleavage, the environment may be conducive to an aspartate-dependent type of autocatalytic mechanism, although Basavappa *et al.* [54] point out that the scissile bond is close to a conserved histidine residue (His2195) in the structure of the poliovirus empty capsid.

The largest and most variable surface loop of VP2 is the 'puff' or EF loop (residues 2129–2180). The puff of CVB3 is six residues shorter than that of PV1/M and three residues longer than that of HRV14. The CVB3 puff consists of two loops: the first (residues 2129–2154) lines the rim of the canyon closest to the twofold axes; the second (residues 2155–2180) sits above the first on the exterior of the virus surface. This exterior region of the puff loop contains NIm sites for polioviruses and rhinoviruses [44–47]. The puff may play a structural role in maintaining the shape and amino acid charge characteristics of the canyon and may be directly or indirectly involved in receptor binding or recognition. In the case of HRV14, residues within the ICAM-1 footprint include residues from the puff loop near the the canyon [17]. In addition, mutational studies of CVB3 have shown that amino acid changes in the puff loop of VP2, especially to regions that line the rim of the canyon and the depression around the twofold axis, often result in non-viable virus (B Coller, J Muckelbauer, M Rossmann and S Tracy, unpublished data).

Table 1. CVB3 residues within 4.0 Å of WIN 66393, palmitate and the VP4–myristate.

WIN 66393				Palmitate				Myristate			
Atom	Distance‡ (Å)	CVB3 residue	CVB3 atom	Atom	Distance‡ (Å)	CVB3 residue	CVB3 atom	Atom	Distance‡ (Å)	CVB3 residue§	CVB3 atom
C51	4.1	Tyr1189	Cδ2	O1	2.6	Arg1095	Nη2	$O1^1$	3.2	$Thr4028^2$	Oγ1
N5	3.4	Pro1094	Cγ	O1	3.1	Arg1095	Nη1	$O1^1$	3.5	$Ile4030^1$	Cδ1
C4	3.9	Pro1094	Cγ	O2	5.8†	Ser1184	Oγ	$C1^1$	3.8	$Thr4028^2$	Oγ1
C3	3.0	Met1213	Cγ	C1	3.7	Arg1095	Nη2	$C2^1$	4.3	$Ala4003^2$	Cβ
C2	3.6	Met1213	Cγ	C2	3.7	Asn1211	Nδ2	$C3^1$	4.8	$Ile4030^1$	Cδ1
N1	3.4	Phe1237	Cε2	C2	3.9	Met1213	Cγ	$C4^1$	4.2	Myr^2	C5
C1#	3.6	Met1213	Cγ	C3	3.8	Pro1094	Cδ	$C5^1$	3.2	Myr^5	C6
C1#	3.8	Ile1092	Cγ2	C4	4.3	Tyr1189	Cε2	$C5^1$	3.8	Myr^5	C5
C2#	3.7	Phe1237	Cζ	C5	4.3	Pro1094	Cδ	$C5^1$	3.8	Myr^2	C5
C2#	3.9	Ile1092	Cγ2	C6	4.4	Phe1237	Cε2	$C6^1$	3.2	Myr^2	C5
C3#	4.2	Phe1237	Cζ	C7	3.6	Met1213	Cγ	$C6^1$	3.6	Myr^2	C6
O1*	3.6	Ile1092	Cδ1	C8	3.9	Ile1092	Cγ2	$C6^1$	3.6	Myr^5	C6
C1*	4.1	Leu1116	Cδ1	C8	4.0	Leu1114	Cδ1	$C7^1$	4.0	$Ile4030^1$	Cδ1
C1*	4.1	Ile1092	Cδ1	C9	4.0	Ile1092	Cγ2	$C8^1$	4.2	Myr^2	C8
C2*	3.9	Tyr1143	Cε2	C10	3.7	Ile1092	Cδ1	$C8^1$	4.2	Myr^5	C8
C3*	3.5	Tyr1143	Cγ	C11	4.0	Ile1092	Cδ1	$C9^1$	4.3	Myr^2	C8
C4*	3.8	Leu1116	Cδ1	C12	3.0	Leu1116	Cδ1	$C10^1$	4.6	$Leu3002^4$	Cδ1
C4*	3.8	Tyr1143	Cβ	C13	3.7	Leu1116	Cδ1	$C11^1$	4.4	$Ile4030^2$	Cβ
C4*	3.8	Leu1116	Cδ1	C14	3.7	Met1178	Cε	$C11^1$	4.5	$Leu3002^4$	Cδ1
C5*	3.5	Leu1116	Cδ1	C14	3.9	Tyr1143	Cβ	$C12^1$	3.6	$Thr4028^2$	O
C5*	3.1	Leu1216	Cδ1	C14	3.9	Leu1116	Cδ1	$C13^1$	3.8	$Leu3002^4$	Cδ1
C6*	3.7	Leu1116	Cδ1	C14	3.9	Leu1216	Cδ1	$C14^1$	4.0	$Thr4028^2$	O
C6*	3.7	Leu1216	Cδ1	C15	3.1	Met1178	Cε				
C21	3.7	Leu1183	Cδ1	C15	3.6	Tyr1143	Cβ				
C21	3.8	Tyr1143	OH	C16	3.0	Met1178	Cε				
I61	3.9	Leu1116	Cδ2								
I61	3.8	Trp1090	Cζ2								
I61	3.0	Leu1216	Cδ2								
N1′	3.3	Tyr1143	Cβ								
N1′	3.6	Met1178	Cε								
N1′	3.7	Pro1165	Cγ								
C2′	3.4	Tyr1143	Cβ								
C2′	3.7	Met1178	Cε								
C2′	4.0	Leu1216	Cδ1								
N3′	3.3	Met1178	Cε								
N3′	3.9	Tyr1143	Cβ								
N3′	3.7	Leu1216	Cδ1								
C4′	2.9	Met1178	Cε								
C4′	4.0	Pro1165	O								
O5′	3.1	Met1178	Cε								
O5′	3.4	Pro1165	Cγ								
O5′	3.7	Tyr1143	Cβ								
C41	3.3	Met1178	Cε								
C41	3.2	Val1167	Cγ2								
C41	3.4	Ser1166	Cα								
C41	3.9	Pro1165	O								

WIN 66393

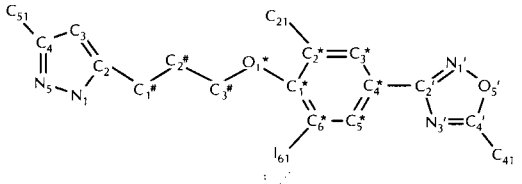

Palmitate

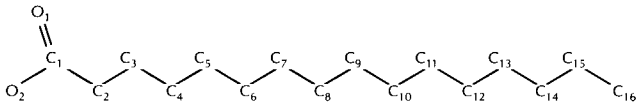

Myristate

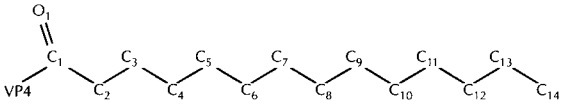

†Possible water-mediated hydrogen bond. ‡Distances greater than 4.0 Å indicate the nearest residue. §The myristate superscripts 1–5 represent the fivefold-symmetry-related myristates and protein numbering scheme where 1 is the reference structure and 2–5 are arranged looking down the fivefold axis towards the viral center in an anticlockwise manner.

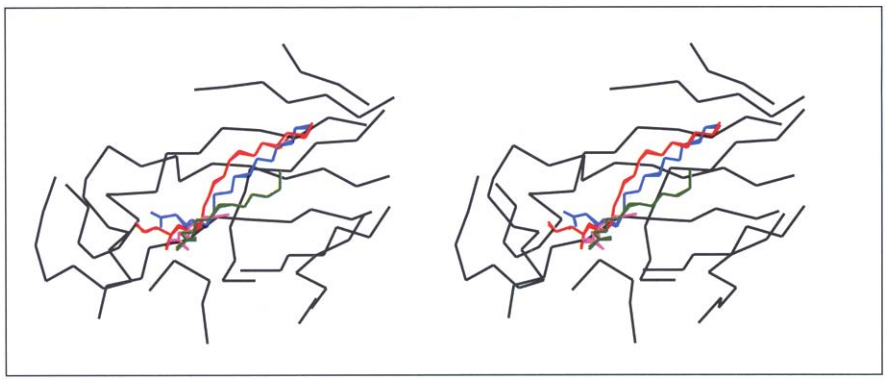

Fig. 3. Pocket factors. Cα backbone structure of the CVB3 VP1 β-sandwich is shown in black with the superpositioned structures of the pocket factors: palmitate (C_{16}) for CVB3 (blue); sphingosine for PV1/M (red); caprate (C_{10}) for HRV16 (green), and caprylate (C_8) for HRV1A (pink).

Lindberg *et al.* [55] have identified two amino acid residues in VP2 that are responsible for the ability of a CVB3 variant (CVB3-RD) to utilize a second receptor on the normally unsusceptible RD cells. One of the residues is Asp2108→Val, which is internal and located on βD. The other residue, Thr2151→Ser, is located on the puff of VP2 and may be involved, directly or indirectly, in receptor recognition. Both valine at 2108 and serine at 2151 are observed for other isolates of CVB3 (Table 2). The isolate, CVB3/Ø, which has serine at position 2151, does not infect RD cells (S Tracy, personal communication), suggesting that this change alone is insufficient to permit RD cell binding.

A thin, plate-like feature of electron density was observed close to residue Trp2038, similar to densities assigned as RNA for HRV14 [56], polioviruses [38] and HRV16 (A Hadfield, M Oliveira and M Rossmann, unpublished data). The density can accommodate a purine base and it appears to make ring-stacking interactions with Trp2038. No other ordered RNA was observed in the CVB3 electron-density map.

Structure of VP3

The N-terminal 25 residues of VP3 are located along the icosahedral fivefold axes at 110 Å from the viral center. The fivefold-symmetry-related N termini form an intertwining β-barrel cylinder (Fig. 4a) whose structure is highly conserved in all picornavirus structures determined so far. This β-cylinder structure is likely to be important in pentamer formation after the release of the VP3 termini by post-translational cleavage [5,6]. Residues 3058–3069 form the knob which is the major surface protrusion of VP3. NIm sites are located on the knob of rhinoviruses and polioviruses [44–47].

Table 2. Amino acid differences in the capsid proteins of CVB3 isolates whose sequences have been published.

CVB3 reference	M*	Nancy [75]	Nancy [73]	20 [76]	Ø [77]	Nancy-RD [55]
VP1						
1023	T	T	N	T	T	T
1045	S	G	G	G	G	G
1080	E	K	E	K	E	K
1092	I	L	L	L	L	L
1180	V	I	I	I	I	I
VP2						
2013	V	A	A	V	A	A
2108	I	V	D	V	V	V
2138	N	D	D	D	D	D
2151	T	T	T	S	S	S
VP3						
3137	P	P	L	P	P	L
3155	V	I	V	V	V	V
3178	Y	F	Y	F	Y	Y
3184	Y	Y	C	Y	Y	Y
3214	V	V	V	V	V	A
3234	E	Q	E	Q	E	Q
VP4						
4016	G	R	G	R	G	G
4030	I	I	I	I	V	I
4051	S	G	G	G	G	G

*CVB3/M was the strain used in the current structural studies.

Structure of VP4

Electron density extending from the N terminus of VP4 was identified as myristate, a C_{14} fatty acid, covalently bound to the N-terminal glycine of VP4 (Fig. 4b). Continuous electron density was observed up to atom C12 of myristate, but the atoms C13 and C14 were missing in the map and presumably assume multiple conformations. The fivefold-related myristates cluster at the interior surface of the virion just below the N-terminal VP3 β-cylinder (Fig. 4a). The myristate mediates interactions between the N termini of VP3 and VP4 and is thought to play an important role in virus assembly by stabilizing pentamers [57]. It has also been suggested that myristate may be involved in disassembly by mediating the association of virus with cellular membranes [58]. The position of the myristate is essentially identical to that found in PV1/M [38]. The carboxylate oxygen of myristate forms a hydrogen bond with a fivefold-symmetry-related side-chain oxygen of Thr4028 (Fig. 4b). It has been shown, by mutagenesis studies, that this interaction is important for normal viral assembly and infectivity in the polioviruses [59]. VP4 meanders from the fivefold axis along the capsid interior to the threefold axis terminating close to the N terminus of VP2.

Surface characteristics

The CVB3 canyon surrounding the icosahedral fivefold axis is not as pronounced as the canyon for the polioviruses and rhinoviruses. It appears to be bridged at the narrowest region of the canyon between VP1 and VP2 (Figs 5,6). The canyon depression of CVB3 (~15 Å deep) is almost coincident with the HRV14 [17] (Fig. 6) and HRV16 (N Olson, P Kolatkar, M Rossmann and T Baker, unpublished data) receptor-binding sites. The extent to which the canyon narrows differs between CVB3, the rhinoviruses and the polioviruses. The residues that make up the bridge are predominantly the C-terminal residues of VP3 along with one or two residues from the EF loop of VP1. For PV1/M, the last three residues of VP3 are disordered and, therefore, their contribution to bridge formation is not observed [6,54]. A second, 15 Å deep, surface depression flanks the icosahedral twofold axes (Figs 5,6). Its floor and walls are lined, predominantly, with residues from VP2 and some from VP3. Residue 2151, one of the two amino acids responsible for the RD phenotype of CVB3-RD (discussed above), projects directly into the twofold depression (shown in Fig. 6 as a surface residue adjacent to the twofold depression) and suggests that this surface depression may serve as a possible receptor-binding site.

Figure 6b shows the conservation of CVB amino acids on the surface of the CVB3 virion. Sequence alignments of CVB1, CVB3, CVB4 and CVB5 (A Palmenberg, personal communication) show that the regions of greatest

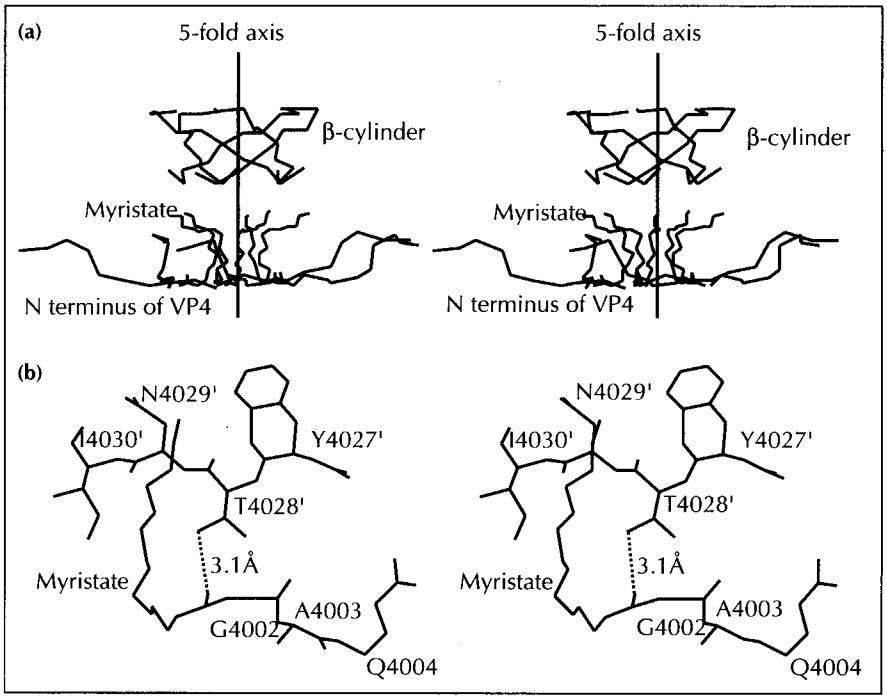

Fig. 4. N terminus of VP4 and myristate. **(a)** View of the fivefold-related myristates and N termini of VP4 near the interior of the virus capsid clustered beneath the VP3 β-cylinder. **(b)** The myristate moiety is shown extending vertically from the terminal glycine of VP4. Also shown is a section of a symmetry-related VP4 (4027′–4030′) showing Thr4028′, which forms a hydrogen bond with the carboxylate oxygen of myristate.

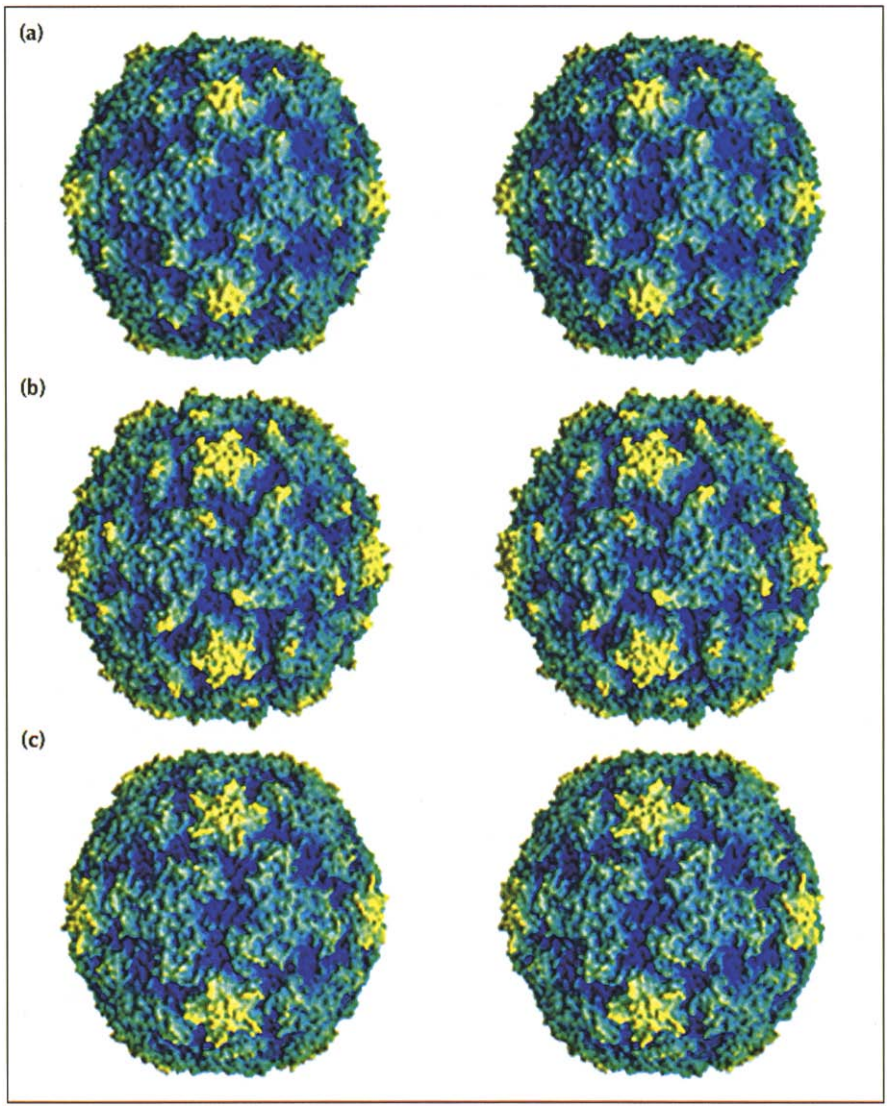

Fig. 5. The water-accessible surfaces. Radial depth-cued images viewed down the icosahedral twofold axis of **(a)** CVB3, **(b)** PV1/M and **(c)** HRV14. Regions of dark blue color represent surface depressions while regions of yellow color represent surface protrusions. (Images courtesy of Jean-Yves Sgro, Institute for Molecular Virology, University of Wisconsin-Madison and created using the program GRASP [78].)

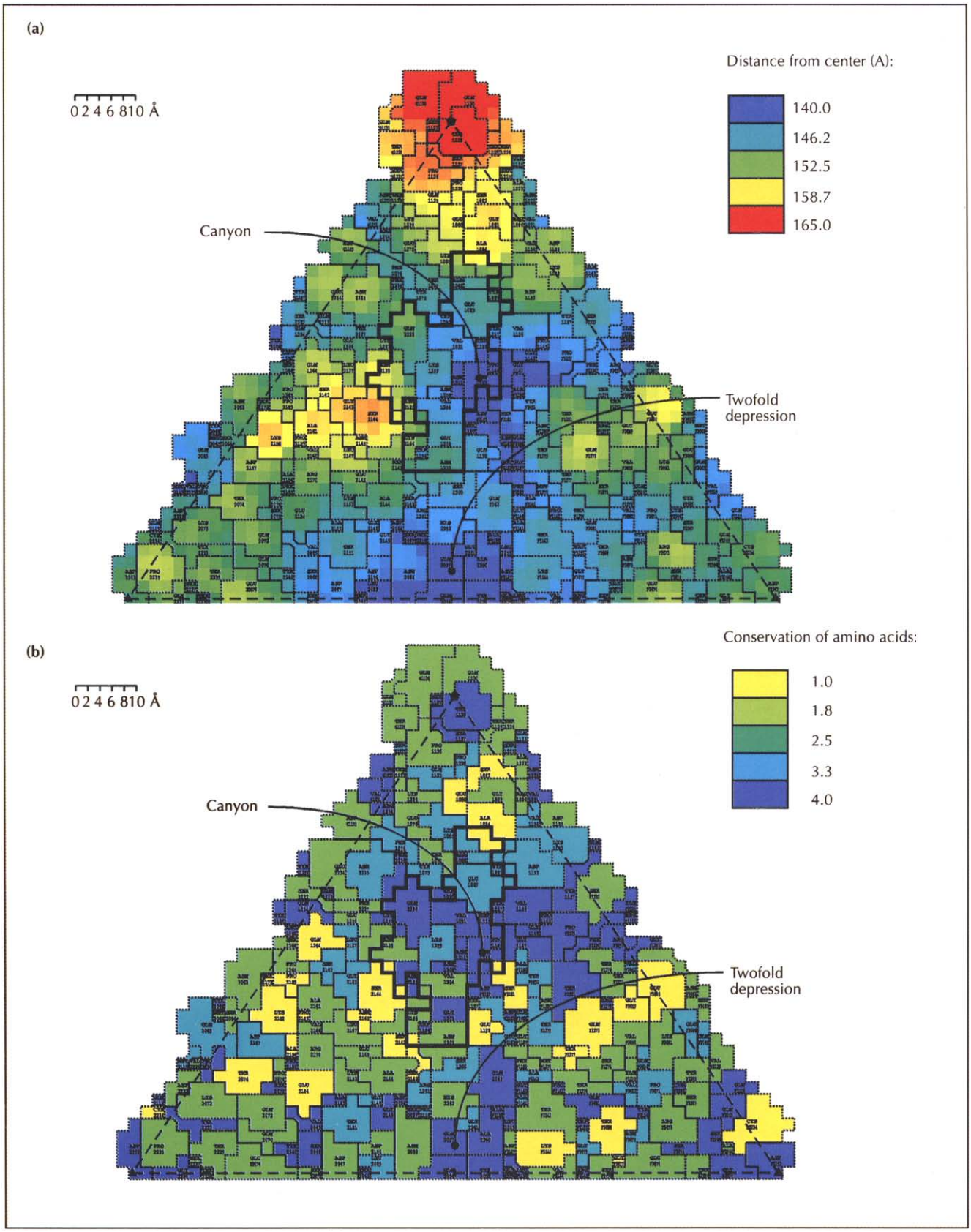

Fig. 6. CVB3 roadmaps. **(a)** An icosahedral asymmetric unit of CVB3 showing the surface residues relative to the distance from the viral center. The depth range is from 140.0–165.0 Å. The thick black outline represents the 'footprint' of residues for HRV14 that are in contact with its viral receptor. **(b)** An icosahedral asymmetric unit of CVB3 showing the conservation of residues for the coxsackie B viruses using CVB1, CVB3, CVB4 and CVB5 sequence alignments (A Palmenberg, personal communication). A score of 4.0 is assigned for a surface residue where all four CVB sequences match, whereas 1.0 is assigned for no matches.

sequence conservation coincide with the canyon surrounding the fivefold axis, and the twofold depression. Amino acids in the canyon of rhinoviruses have been shown to be the most conserved surface amino acids [19,20]. The conservation of amino acids for the CVBs in the canyon and, to a lesser extent, in the twofold depression supports the hypothesis that the canyon and/or the twofold depression are receptor-binding sites. The more extensive conservation of residues in the canyon as opposed to that in the twofold depression may distinguish the canyon as the major receptor-binding site for all six CVB serotypes, whereas the twofold depression may function as an alternative or second receptor site.

In addition to identifying conserved regions on the surface of the CVBs, regions with no conservation were also identified (Fig. 6b). These sites, which correspond to variable loops and C termini on the extreme surface of the virus, are analogous to NIm sites for the polioviruses and rhinoviruses and may also contain NIm sites for CVB3 and other CVBs.

Water molecules and ions

The assignment of water molecules throughout the structure was not attempted at 3.5 Å resolution. However, regions of the map, namely along the fivefold and threefold axes and in the drug-binding pocket, showed peaks of electron density that could reasonably be attributed to water and were tentatively assigned as such.

Unidentified density, twice the height of the surrounding protein density, was observed on the icosahedral threefold axis at the outer surface of the virion, approximately 148 Å from the viral center (Fig. 7a). Using EGTA-soaking experiments, similar density observed for HRV14 has recently been shown to be Ca^{2+} coordinated to Glu3200 (R Zhao and M Rossmann, unpublished data). Although soaking experiments with EGTA have not been carried out for CVB3, we propose that the observed density on the threefold axis is also Ca^{2+}. Bidentate coordination (~2.5 Å distances) occurs with the six side-chain oxygens of threefold-related aspartic acids (Asp3203). An additional ligand to a water molecule occurs directly below the Ca^{2+}, closer to the viral center on the threefold axis. Residue 3203 is conserved among the CVBs as aspartic or glutamic acid, suggesting that all CVBs may bind Ca^{2+} at this position. However, the trend of conservation does not hold for all rhinoviruses and enteroviruses and, hence, the threefold Ca^{2+} site for the picornaviruses is not ubiquitous.

Two peaks of electron density were observed on the fivefold axis at 153 Å and 147 Å from the viral center. These are also proposed to be ion-binding sites (Fig. 7b). These peaks, approximately 75% of the height of the surrounding protein electron density, appear to make water-mediated interactions with the side-chain oxygen of Asp1133 and with the main-chain oxygen of Gln1132. Residue Asp1133 is conserved as aspartic acid for the CVBs and both Asp1133 and Gln1132 are located on the DE loop (discussed above) of VP1. The density of these peaks is weaker than the threefold ion peak and is poorly defined, suggesting that the sites on the fivefold axis are not as well occupied as the putative Ca^{2+} site on the threefold

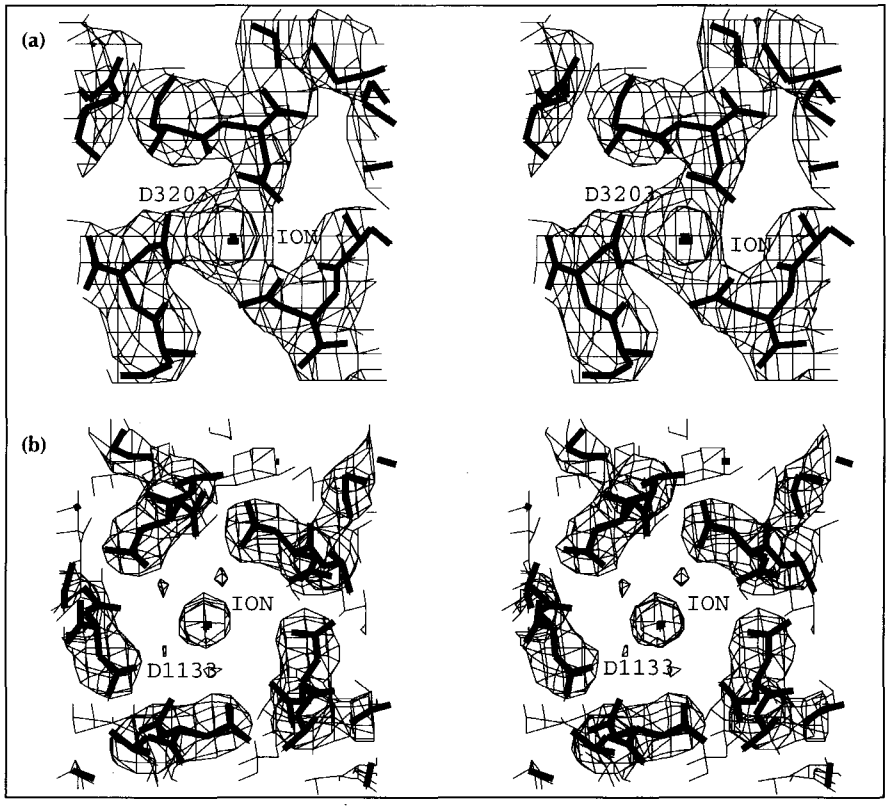

Fig. 7. Stereoviews of the electron density for the putative **(a)** threefold and **(b)** fivefold ions of CVB3 viewed down the relevant axis towards the viral center. In (a), the putative Ca^{2+} appears to be coordinated by threefold-related aspartic acids (Asp3203) on VP3. In (b), the ion, at 153 Å from the viral center, appears to make water-mediated interactions with fivefold-related aspartic acids (Asp1133) on VP1.

axis. The peak at 153 Å corresponds to the putative ion-binding site previously observed for HRV14, Mengo virus, HRV1A and HRV16 [5,7,36,39]. The same EGTA-soaking experiments that identified Ca^{2+} on the threefold axis of HRV14 also identified Ca^{2+} at the fivefold ion site (R Zhao and M Rossmann, unpublished data). For HRV14 the level of occupancy of the fivefold ion site appears to be variable, depending on pH or the absence or presence of antiviral compounds ([60]; M Rossmann, unpublished data). The Ca^{2+} may bind to the rhinoviruses on account of its presence in the crystallization solution or, alternatively, it may bind during the assembly process. For CVB3, the purification and crystallization solutions do not contain Ca^{2+} and crystallization is from NaCl. The favorable protein environment for ion binding and the analogous ions observed for other picornaviruses suggests that CVB3 can bind a cation at the fivefold site.

Bacteriophage ϕX174 binds Ca^{2+} on the fivefold and threefold axes, in addition to a site off the threefold axis [61,62]. For ϕX174, the binding of Ca^{2+} initiates the ejection of DNA through the fivefold vertex in the early stages of the phage life cycle [63,64]. Kalko *et al.* [65] demonstrated how the fivefold axes for some icosahedral viruses are reminiscent of channel-like ion-binding and ion-transport proteins. The superposition of the fivefold axes and ion-binding sites of CVB3 and ϕX174 revealed similar channel-like structures along the fivefold axis (Fig. 8). The amino acids that line the fivefold channel for CVB3 are polar, with a high predominance of glutamine, asparagine and glutamic acid residues in the vicinity of the ion-binding site and near the exterior surface of the capsid. These channels may be involved in important early steps of viral disassembly. Indeed, acid-induced conformational changes of the GH loop of VP1 and the fivefold β-cylinder of VP3 plus loss of the Ca^{2+} from the fivefold axis in HRV14 [60] suggest that the fivefold channels are important in disassembly. However, Flore *et al.* [66] propose the occurrence of a different set of conformational changes in the formation of poliovirus 'A' particles in the early stages of uncoating, while intact pentamers may be intermediates in the disassembly of aphthoviruses [67] and cardioviruses [68].

The N terminus of VP1 is disordered in CVB3, polioviruses and rhinoviruses, to a greater or lesser extent. In many cases, however, sequences in this region of VP1 display amphipathic helical character [66] showing that the amino acid sequence is prone to helix formation. This part of the structure is subject to externalization during the early stages of infection [42]. The variable nature of this structure and its sequence preference for helicity might suggest that the infection process requires a major conformational change involving the amphipathic helix, possibly by a mechanism similar to the conformational changes observed for influenza virus hemagglutinin in the process of membrane fusion [69].

Antiviral compound

The antiviral compound, WIN 66393 (synthesized by SWPRD), was used for CVB3 crystal-soaking studies. WIN compounds do not inhibit CVB3 attachment to monkey kidney cells but act by inhibiting viral uncoating (P Fox, G Diana, F Dutko, J Groarke, D Pevear, unpublished data). WIN 66393 is iodinated on the phenyl ring (Table 1) and was used as a potential heavy-atom marker for crystallographic experiments performed in an attempt to solve positioning, orienting and packing ambiguities for CVB3 particles described elsewhere [70].

WIN 66393 binds into the hydrophobic β-sandwich pocket of VP1 (Fig. 2b). Amino acid residues in the pocket close to the drug are predominately hydrophobic (Table 1). The main-chain oxygen of Pro1165 at the interior end of the pocket and the hydroxyl group of Try1143 are the only two polar atoms within 4.0 Å of WIN 66393. Conformational changes upon drug binding are minimal because the pocket is occupied in its native state by the pocket factor. As WIN 66393 is considerably shorter than the native pocket factor, the absence of pocket factor at the ends of the VP1 pocket indicate that the antiviral compound displaced the pocket factor completely (compare Fig. 2a,b). There is some indication that Ile1092 moves (by ~1.0 Å) to accommodate the substituted phenyl ring on the WIN compound. In light of the small conformational changes in the pocket and the overlying canyon on the binding of WIN 66393, it is not surprising that receptor attachment is not inhibited

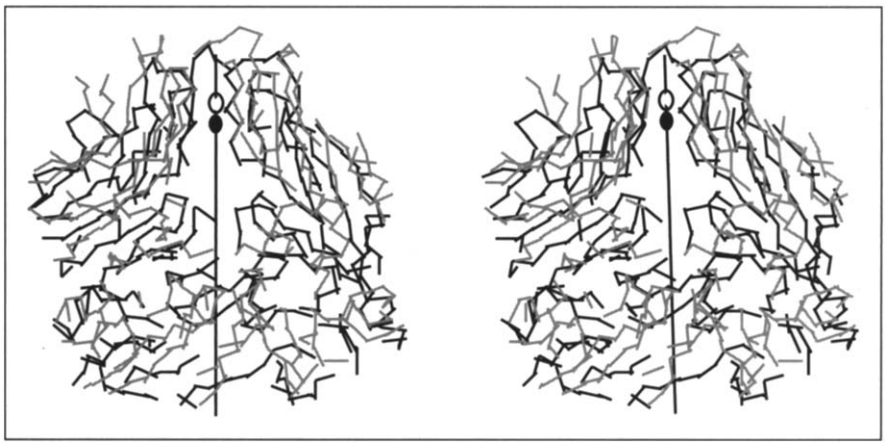

Fig. 8. Fivefold channels. Cα backbone superposition matching the viral centers and icosahedral axes of CVB3 (black) and ϕX174 (gray). The view is perpendicular to the fivefold axis (black vertical line) showing the channel formed along this axis. The dots on the fivefold axis show the positions of the ions for CVB3 (filled dot) and ϕX174 (open dot), respectively.

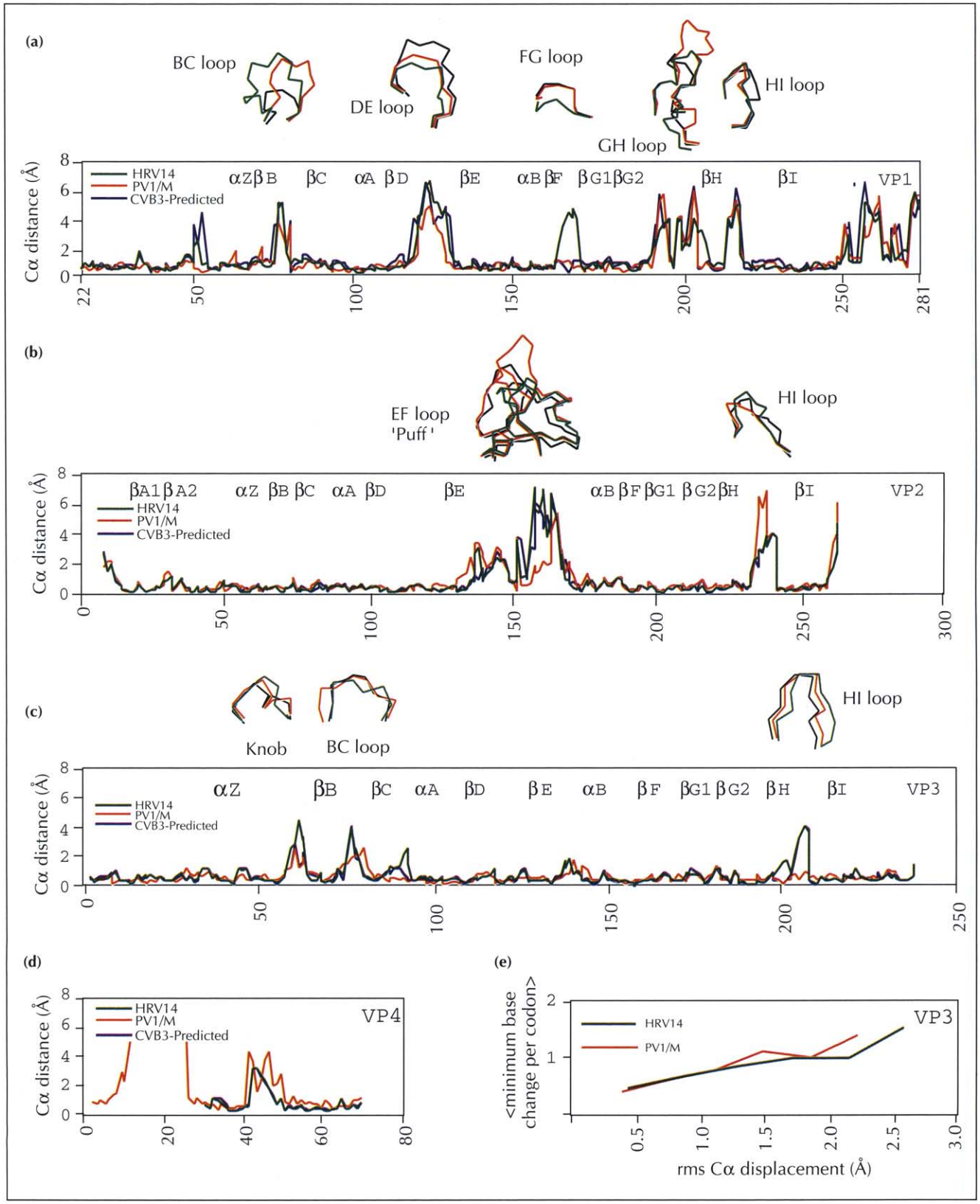

Fig. 9. Structural comparisons of CVB3 with PV1/M, HRV14 and a predicted CVB3 structure [72]. Plots of Cα distances *versus* CVB3 amino acid sequence for aligned structures of CVB3 with PV1/M, HRV14 and a predicted CVB3 structure are shown for **(a)** VP1, **(b)** VP2, **(c)** VP3 and **(d)** VP4. Above plots (a–c) are the Cα structures of regions which show the most differences in structure. The CVB3 structure is shown in black with PV1/M in red and HRV14 in green. The predicted CVB3 loop structures are not shown. **(e)** The deviation (in Å) of Cα atoms for PV1/M and HRV14 from equivalent positions in CVB3 VP3 were plotted against the average minimum base change per codon. The size of the Cα deviation correlates well with the number of nucleic acid base changes. Similar plots were obtained for VP1 and VP2 (not shown).

Fig. 10. Sequence alignments of CVB3, PV1/M and HRV14 for **(a)** VP1, **(b)** VP2, **(c)** VP3 and **(d)** VP4. The numbering shown is for the CVB3 sequence. Secondary structural elements (for a definition see [5]) are shown above the sequences. Capital letters denote identical residues for the sequences shown. Underlined residues indicate surface residues for CVB3. Bold-faced type indicates residues that line the β-sandwich pocket of VP1.

(assuming that the canyon is the receptor-binding site). Moreover, if the receptor-binding site were elsewhere, the WIN compound would also fail to inhibit attachment.

WIN compounds with substituted phenyl rings, that were active against CVB3/M, were found to be inactive against CVB3-Nancy (P Fox, G Diana, F Dutko, J Groarke, D Pevear and T Woods, unpublished data). There are two residues (1092 and 1180) located in the WIN pocket that differ between CVB3/M and various isolates of CVB3-Nancy (Table 2). For CVB3-Nancy, residue 1092 is a leucine instead of an isoleucine and residue 1180 is an isoleucine instead of a valine. Moreover, for the rhinoviruses and enteroviruses, residue 1092 is conserved as isoleucine and residue 1180 is conservatively hydrophobic (valine, leucine or isoleucine). These two residues are situated across the pocket from each other with their side chains extending into the pocket (Fig. 2) and both are near the substituted phenyl ring of the WIN compound. For CVB3-Nancy, the change from isoleucine to leucine at 1092, in addition to Val1180→Ile, may be responsible for the inability of the virus to bind WIN compounds. By filling the pocket with bulkier side chains, these residues may block the binding of drugs in an analogous way to the exclusion mutants of HRV14 [32]. This is supported by the fact that WIN compounds with unsubstituted phenyl rings do not differentiate between CVB3/M and CVB3-Nancy (G Diana, F Dutko, J Groarke and D Pevear, unpublished data).

Similarity to other picornaviruses

Structural comparisons between the coat proteins of CVB3 and other picornavirus structures were performed using methods developed by Rossmann and Argos [71]. Figure 9a–d shows plots of differences in Cα positions for VP1, VP2, VP3 and VP4 when CVB3 was superimposed on PV1/M and HRV14. The degree of amino acid conservation, expressed as the average minimum base change, corresponds to the degree of structural similarity (measured by the root mean square [rms] displacement of Cα atoms; Fig. 9e). Regions with differences less than 1σ in the deviation of Cα positions correspond to the β-strands of the conserved β-sandwich. However, many loops between the β-strands displayed differences of up to 7 Å. These are located mostly on the external surfaces and correspond to regions with the greatest sequence variability (Fig. 10). Above each plot (Fig. 9a–c) is a Cα tracing of the regions with greatest structural difference which represent parts of the virus structure that alter viral characteristics such as receptor specificity, antigenicity and stability. Of the three major coat proteins, VP1 shows the most structural diversity and has the lowest percentage sequence identity of the coat protein subunits (Table 3), whereas VP3 exhibits the most structural and sequence similarity. CVB3 shares higher sequence identity with the polioviruses than with the rhinoviruses (Table 3). For VP1, HRV14 differs most from CVB3 at the fivefold loops (BC, DE, FG) whereas PV1/M differs most from CVB3 at the GH loop lining the canyon (Fig. 9a). For VP2, while the N and C termini of CVB3 differ slightly from PV1/M and HRV14, the major regions of difference are the puff (EF loop) and HI loop (Fig. 9b). For VP3, the major regions of difference are the knob, the BC loop and the HI loop (Fig. 9c).

Table 3. Percentage amino acid sequence identities of aligned capsid proteins for selected enteroviruses and rhinoviruses.*

	CVB3 *versus* PV1/M	CVB3 *versus* HRV14	PV1/M *versus* HRV14
VP1	46	37	42
VP2	56	55	54
VP3	56	49	42
VP4	66	60	57

*Amino acid sequences and alignments were obtained from A Palmenberg (personal communication). Percentage amino acid identities were calculated as the (number of matches/average length of the compared pair)×100 [4].

Predicted *versus* crystallographic structure of CVB3

Liljas *et al.* [72] predicted the three-dimensional structure of CVB3-Nancy based on the structures of HRV14 and PV1/M and the amino acid sequence of CVB3-Nancy [73]. Figure 9a–d includes the predicted structure of CVB3 where it is compared with the actual X-ray crystallographic structure. The β-sheet loops and termini were the major regions of difference between the predicted and actual CVB3 structures, which are also the sites of the major differences described for PV1/M and HRV14. The predicted structure of CVB3 is about as different from the actual CVB3 structure as PV1/M is from CVB3 and, not surprisingly, is least accurate in the regions of the structure that are most variable and functionally unique.

Biological implications

The six serotypes of coxsackie B viruses (CVBs) cause a number of human illnesses that range in severity from paralysis and death to asymptomatic infections. CVBs have been recognized as the major viral agents causing myocarditis in adults and children. The ability of the CVBs to infect different tissues and cause disease may be related to structural changes that take place on the surface of the virus or in the protein capsid shell. These changes may affect cellular recognition and may allow the virus to utilize a variety of receptors and, as a consequence, infect a number of different tissues.

Earlier results have shown that there are at least two different receptors that CVB3 can use for cell entry, an observation that may have important implications for viral pathogenesis. One of the CVB3 receptors is the same cell-surface molecule that is used by some adenovirus serotypes. Shape, amino acid charge, amino acid conservation, CVB variants and comparison with rhinovirus and poliovirus structures suggest that the surface depression around the icosahedral fivefold axes (the canyon), which is the site of receptor attachment for the rhinoviruses and enteroviruses, and the depression at the twofold axes are possible sites of cell attachment.

CVBs, like polioviruses, but in contrast to the rhinoviruses, are stable at acid pH. This stability may be partly attributable to the presence of a large pocket factor (of cellular origin that binds into the VP1 β-sandwich) and may also be influenced by the ion-binding sites on the icosahedral threefold and fivefold axes. Comparisons between CVB3 and other viruses of the ion-binding sites and the residues lining the icosahedral fivefold channels suggest that this may be a route for the externalization of the N terminus of VP1, VP4 and possibly the nucleic acid genome in the early stages of viral infection.

Complexes of CVB3 with an antiviral compound show that such compounds can displace the pocket factors under conditions used crystallographically and that there is nearly full occupancy of the pocket factors in the virus. The presence of particular amino acid residues lining the pocket can be correlated with the effective range of the antiviral agents.

Materials and methods

Crystallography

The crystal structure of CVB3 and its complex with an antiviral compound were determined to 3.5 Å resolution [70]. CVB3 was purified by a modified procedure of Mapoles *et al.* [23] and crystallized at room temperature using 0.75 M NaCl as precipitant. X-ray diffraction data were collected at the Cornell High Energy Synchrotron Source (CHESS) on the F1 station. The CVB3 particles crystallized in a pseudo R32 space group, although the true space group was $P2_1$ (a=574.6 Å, b=302.1 Å, c=521.6 Å, β=107.7°) with two virions in the asymmetric unit giving 120-fold non-crystallographic redundancy. The crystals diffracted to 2.7 Å resolution and the X-ray data set was 55% complete to 3.0 Å resolution with an R-merge of 12.8% [70]. Real-space electron-density averaging and solvent flattening were performed using HRV14 as an initial phasing model. A structural model was built and partially refined to 3.5 Å resolution. The R-factor for the present model, not including water molecules, ions, pocket factor or the N-terminal myristate on VP4, is 26.4%. The rms deviations in bond distances and bond angles are 0.013 Å and 1.8°, respectively. Coordinates for CVB3 coat protein have been deposited in the Brookhaven Protein Data Bank (1COV).

CVB3 amino acid sequence

The strain of CVB3 for which the structure was solved is the M strain originally characterized by Gauntt *et al.* [74]. The amino acid sequence of the capsid protein of CVB3/M was provided by Dr Steven Tracy, University of Nebraska Medical Center at Omaha and Dr Charles Gauntt, University of Texas Health Science Center at San Antonio. Sequence alignments of the capsid proteins for CVB3/M, HRV14 and PV1/M (Fig. 10) were based on structural superpositions and they agree well with sequence alignments [4], with some differences in loop regions. Sequence differences between CVB3/M and other isolates of CVB3 are listed in Table 2.

Acknowledgements: We gratefully acknowledge Steven Tracy and Charles Gauntt for the amino acid sequence of the CVB3/M isolate, Lars Liljas for the predicted CVB3 structure coordinates, Andrea Hadfield for the HRV16 pocket factor coordinates and Rob McKenna for the ϕX174 coordinates. We would like to thank Jean-Yves Sgro, Institute for Molecular Virology, University of Wisconsin-Madison, for creating beautiful figures as shown in Figure 5 and Tom Smith for his help creating many of the figures. This work was funded by grants to MGR from the National Institutes of Health and Sterling Winthrop Pharmaceuticals Research Division.

References

1. Rueckert, R.R. (1990). Picornaviridae and their replication. In *Virology*. (2nd edn) (Fields, B. & Knipe, D., eds), pp. 507–548, Raven Press Ltd., New York.
2. Caspar, D.L.D. & Klug, A. (1962). Physical principles in the construction of regular viruses. *Cold Spring Harb. Symp. Quant. Biol.* **27**, 1–24.
3. Melnick, J.L. (1990). Enteroviruses: polioviruses, coxsackieviruses, echoviruses and newer enteroviruses. In *Virology*. (2nd edn) (Fields, B. & Knipe, D., eds), pp. 549–605, Raven Press Ltd., New York.
4. Palmenberg, A.C. (1989). Sequence alignments of picornaviral capsid proteins. In *Molecular Aspects of Picornavirus Infection and Detection*. (Semler, B.L. & Ehrenfeld, E., eds), pp. 211–241, American Society for Microbiology, Washington, DC.
5. Rossmann, M.G., *et al.*, & Vriend, G. (1985). Structure of a human common cold virus and functional relationship to other picornaviruses. *Nature* **317**, 145–156.
6. Hogle, J.M., Chow, M. & Filman, D.J. (1985). Three-dimensional structure of poliovirus at 2.9 Å resolution. *Science* **229**, 1358–1365.
7. Luo, M., *et al.*, & Palmenberg, A. (1987). The atomic structure of Mengo virus at 3.0 Å resolution. *Science* **235**, 182–191.
8. Acharya, R., Fry, E., Stuart, D., Fox, G., Rowlands, D. & Brown, F. (1989). The three-dimensional structure of foot-and-mouth disease virus at 2.9 Å resolution. *Nature* **337**, 709–716.
9. Greve, J.M., *et al.*, & McClelland, A. (1989). The major human rhinovirus receptor is ICAM-1. *Cell* **56**, 839–847.
10. Staunton, D.E., Merluzzi, V.J., Rothlein, R., Barton, R., Marlin, S.D. & Springer, T.A. (1989). A cell adhesion molecule, ICAM-1, is the major surface receptor for rhinoviruses. *Cell* **56**, 849–853.
11. Huber, S. (1994). VCAM-1 is a receptor for encephalomyocarditis virus on murine vascular endothelial cells. *J. Virol.* **68**, 3453–3458.
12. Mendelsohn, C.L., Wimmer, E. & Racaniello, V.R. (1989). Cellular receptor for poliovirus: molecular cloning, nucleotide sequence, and expression of a new member of the immunoglobulin superfamily. *Cell* **56**, 855–865.
13. Hofer, F., *et al.*, & Blass, D. (1994). Members of the low density lipoprotein receptor family mediate cell entry of a minor group common cold virus. *Proc. Natl. Acad. Sci. USA* **91**, 1839–1842.
14. Bergelson, J.M., Shepley, M.P., Chan, B.M.C., Hemler, M.E. & Finberg, R.W. (1992). Identification of the integrin VLA-2 as a receptor for echovirus 1. *Science* **255**, 1718–1720.
15. Bergelson, J.M., Chan, M., Solomon, K.R., St. John, N.F., Lin, H. & Finberg, R.W. (1994). Decay-accelerating factor (CD55), a glycosylphosphatidylinositol-anchored complement regulatory protein, is a receptor for several echoviruses. *Proc. Natl. Acad. Sci. USA* **92**, 6245–6248.
16. Ward, T., Pipkin, P.A., Clarkson, N.A., Stone, D.M., Minor, P.D. & Almond, J.W. (1994). Decay-accelerating factor CD55 is identified as the receptor for echovirus 7 using CELICS, a rapid immuno-focal cloning method. *EMBO J.* **13**, 5070–5074.
17. Olson, N.H., *et al.*, & Rossmann, M.G. (1993). Structure of a human rhinovirus complexed with its receptor molecule. *Proc. Natl. Acad. Sci. USA* **90**, 507–511.
18. Rossmann, M.G. (1989). The canyon hypothesis. *J. Biol. Chem.* **264**, 14587–14590.
19. Rossmann, M.G. & Palmenberg, A.C. (1988). Conservation of the putative receptor attachment site in picornaviruses. *Virology* **164**, 373–382.
20. Chapman, M.S. & Rossmann, M.G. (1993). Comparison of surface properties of picornaviruses: strategies for hiding the receptor site from immune surveillance. *Virology* **195**, 745–756.
21. Colonno, R.J., Condra, J.H., Mizutani, S., Callahan, P.L., Davies, M. & Murcko, M.A. (1988). Evidence for the direct involvement of the rhinovirus canyon in receptor binding. *Proc. Natl. Acad. Sci. USA* **85**, 5449–5453.
22. Colston, E. & Racaniello, V.R. (1994). Soluble receptor-resistant poliovirus mutants identify surface and internal capsid residues that control interaction with the cell receptor. *EMBO J.* **13**, 5855–5862.
23. Mapoles, J.E., Krah, D.L. & Crowell, R.L. (1985). Purification of a HeLa cell receptor protein for the group B coxsackieviruses. *J. Virol.* **55**, 560–566.
24. Hsu, K.L., Paglini, S., Alstein, B. & Crowell, R.L. (1990). Identification of a second cellular receptor for a coxsackievirus B3 variant, CVB3-RD. In *New Aspects of Positive Strand RNA Viruses*. (Brinton, M.A. & Heinz, F.X., eds), pp. 271–277, American Society for Microbiology, Washington, DC.
25. Bergelson, J.M., Mohanty, J.G., Crowell, R.L., St. John, N., Lublin, D.M. & Finberg, R.W. (1995). Coxsackievirus B3 adapted to growth in RD cells binds to decay-accelerating factor (CD55). *J. Virol.* **69**, 1903–1906.
26. Reagan, K.J., Goldberg, G. & Crowell, R.L. (1984). Altered receptor specificity of coxsackievirus B3 after growth in rhabdomyosarcoma cells. *J. Virol.* **49**, 635–640.
27. Lonberg-Holm, K., Crowell, R.L., & Philipson, L. (1976). Unrelated animal viruses share receptors. *Nature* **259**, 679–681.
28. Xia, D., Henry, L.J., Gerard, R.D. & Deisenhofer, J. (1994). Crystal structure of the receptor-binding domain of adenovirus type 5 fiber protein at 1.7 Å resolution. *Structure* **2**, 1259–1270.
29. Zhang, A., *et al.*, & Arnold. E. (1993). Structure determination of antiviral compound SCH 38057 complexed with human rhinovirus 14. *J. Mol. Biol.* **230**, 857–867.
30. Fox, M.P., Otto, M.J. & McKinlay, M.A. (1986). The prevention of rhinovirus and poliovirus uncoating by WIN 51711: a new antiviral drug. *Antimicrob. Agents Chemother.* **30**, 110–116.
31. Pevear, D.C., *et al.*, & Dutko, F.J. (1989). Conformational changes in the floor of the human rhinovirus canyon blocks adsorption to HeLa cell receptors. *J. Virol.* **63**, 2202–2207.
32. Heinz, B.A., Shepard, D.A & Rueckert, R.R. (1990). Escape mutant analysis of a drug-binding site can be used to map functions in the rhinovirus capsid. In *Use of X-ray Crystallography in the Design of Antiviral Agents*. (Laver, W.G. & Air, G.M., eds), pp. 173–185, Academic Press Inc., New York.

33. Smith, T.J., *et al.*, & Otto, M.J. (1986). The site of attachment in human rhinovirus 14 for antiviral agents that inhibit uncoating. *Science* **233**, 1286–1293.
34. Badger, J., Minor, I., Oliveira, M.A., Smith, T.J. & Rossmann, M.G. (1989). Structural analysis of antiviral agents that interact with the capsid of human rhinoviruses. *Proteins* **6**, 1–19.
35. Kim, K.H., *et al.*, & Rossmann, M.G. (1993). A comparison of the anti-rhinoviral drug binding pocket in HRV14 and HRV1A. *J. Mol. Biol.* **230**, 206–227.
36. Oliveira, M.A., *et al.*, & Rossmann, M.G. (1993). The structure of human rhinovirus 16. *Structure* **1**, 51–68.
37. Grant, R.A., Hiremath, C.N., Filman, D.F., Syed, R., Andries, K. & Hogle, J.M. (1994). Structures of poliovirus complexes with anti-viral drugs: implications for viral stability and drug design. *Curr. Biol.* **4**, 784–797.
38. Filman, D.J., Syed, R., Chow, M., Macadam, A.J., Minor, P.D. & Hogle, J. (1989). Structural factors that control conformational transitions and serotype specificity in type 3 poliovirus. *EMBO J.* **8**, 1567–1579.
39. Kim, S., *et al.*, & McKinlay, M.A. (1989). The crystal structure of human rhinovirus serotype 1A (HRV1A). *J. Mol. Biol.* **210**, 91–111.
40. Chelvanayagam, G., Heringa, J. & Argos, P. (1992). Anatomy and evolution of proteins displaying the viral capsid jellyroll topology. *J. Mol. Biol.* **228**, 220–242.
41. McGeady, M.L. & Crowell, R.L. (1981). Proteolytic cleavage of VP1 in 'A' particles of coxsackievirus B3 does not appear to mediate virus uncoating by HeLa cells. *J. Gen. Virol.* **55**, 439–450.
42. Fricks, C.E. & Hogle, J.M. (1990). Cell-induced conformational change in poliovirus: externalization of the amino terminus of VP1 is responsible for liposome binding. *J. Virol.* **64**, 1934–1945.
43. Caggana, M., Chan, P. & Ramsingh, A. (1993). Identification of a single amino acid residue in the capsid protein VP1 of coxsackievirus B4 that determines the virulent phenotype. *J. Virol.* **67**, 4797–4803.
44. Sherry, B. & Rueckert, R.R. (1985). Evidence for at least two dominant neutralization antigens on human rhinovirus 14. *J. Virol.* **53**, 137–143.
45. Sherry, B., Mosser, A.G., Colonno, R.J. & Rueckert, R.R. (1986). Use of monoclonal antibodies to identify four neutralization immunogens on a common cold picornavirus, human rhinovirus 14. *J. Virol.* **57**, 246–257.
46. Minor, P.D., Ferguson, M., Evans, D.M., Almond, J.W. & Icenogle, J.P. (1986). Antigenic structure of polioviruses of serotypes 1, 2 and 3. *J. Gen. Virol.* **67**, 1283–1291.
47. Page, G.S., Mosser, A.G., Hogle, J.M., Filman, D.J., Rueckert, R.R. & Chow, M. (1988). Three-dimensional structure of poliovirus serotype 1 neutralizing determinants. *J. Virol.* **63**, 1781–1794.
48. Reimann, B.Y., Zell, R. & Kandolf, R. (1991). Mapping of a neutralizing antigenic site of coxsackievirus B4 by construction of an antigen chimera. *J. Virol.* **65**, 3475–3480.
49. Murray, M.G., Bradley, J., Yang, X.F., Wimmer, E., Moss, E.G. & Racaniello, V.R. (1988). Poliovirus host range is determined by a short amino acid sequence in neutralizing antigenic site 1. *Science* **241**, 213–215.
50. Arnold, E., *et al.*, & Wimmer, E. (1987). Implications of the picornavirus capsid structure for polyprotein processing. *Proc. Natl. Acad. Sci. USA* **84**, 21–25.
51. Harber, J.J., Bradley, J., Anderson, C.W. & Wimmer, E. (1991). Catalysis of poliovirus VP0 maturation cleavage is not mediated by serine 10 of VP2. *J. Virol.* **65**, 326–334.
52. Lee, W.M., Monroe, S.S. & Rueckert, R.R. (1993). Role of maturation cleavage in infectivity of picornaviruses: activation of an infectosome. *J. Virol.* **67**, 2110–2122.
53. Zlotnick, A., *et al.*, & Johnson, J.E. (1994). Capsid assembly in a family of animal viruses primes an autoproteolytic maturation that depends on a single aspartic acid residue. *J. Biol. Chem.* **269**, 13680–13684.
54. Basavappa, R., Syed, R., Flore, O., Icenogle, J.P., Filman, D.J. & Hogle, J.M. (1994). Role and mechanism of the maturation cleavage of VP0 in poliovirus assembly: structure of the empty capsid assembly intermediate at 2.9 Å resolution. *Protein Sci.* **3**, 1651–1669.
55. Lindberg, M.A., Crowell, R.L., Zell, R., Kandolf, R. & Pettersson, U. (1992). Mapping of the RD phenotype of the Nancy strain of coxsackievirus B3. *Virus Res.* **24**, 187–196.
56. Arnold, E. & Rossmann, M.G. (1990). Analysis of the structure of a common cold virus, human rhinovirus 14, refined at a resolution of 3.0 Å. *J. Mol. Biol.* **211**, 763–801.
57. Ansardi, D.C., Porter, D.C. & Morrow, C.D. (1992). Myristylation of poliovirus capsid precursor P1 is required for assembly of subviral particles. *J. Virol.* **66**, 4556–4563.
58. Chow, M., Newman, J.F.E., Filman, D., Hogle, J.M., Rowlands, D.J. & Brown, F. (1987). Myristylation of picornavirus capsid protein VP4 and its structural significance. *Nature* **327**, 482–486.
59. Moscufo, N. & Chow, M. (1992). Myristate–protein interactions in poliovirus: interactions of VP4 threonine 28 contribute to the structural conformation of assembly intermediates and the stability of assembled virions. *J. Virol.* **66**, 6849–6857.
60. Giranda, V.L., *et al.*, & Rueckert, R.R. (1992). Acid-induced structural changes in human rhinovirus 14: possible role in uncoating. *Proc. Natl. Acad. Sci. USA* **89**, 10213–10217.
61. McKenna, R., *et al.*, & Incardona, N.L. (1992). Atomic structure of single-stranded DNA bacteriophage ϕX174 and its functional implications. *Nature* **355**, 137–143.
62. Ilag, L.L., McKenna, R., Yadav, M.P., BeMiller, J.N., Incardona, N.L. & Rossmann, M.G. (1994). Calcium ion-induced structural changes in bacteriophage ϕX174. *J. Mol. Biol.* **244**, 291–300.
63. Incardona, N.L. & Selvidge, L. (1973). Mechanism of adsorption and eclipse of bacteriophage ϕX174. II. Attachment and eclipse with isolated *Escherichia coli* cell wall lipopolysaccharide. *J. Virol.* **11**, 775–782.
64. Yazaki, K. (1981). Electron microscopic studies of bacteriophage ϕX174 intact and 'eclipsing' particles, and the genome by the staining and shadowing method. *J. Virol Methods* **2**, 159–167.
65. Kalko, S.G., Cachau, R.E. & Silva, A.M. (1992). Ion channels in icosahedral virus: a comparative analysis of the structures and binding sites at their fivefold axes. *Biophys. J.* **63**, 1133–1145.
66. Flore, O., Fricks, C.E., Filman, D.J. & Hogle, J.M. (1990). Conformational changes in poliovirus assembly and cell entry. *Semin. Virol.* **1**, 429–438.
67. Logan, D., *et al.*, & Fry, E. (1993). Structure of a major immunogenic site on foot-and-mouth disease virus. *Nature* **362**, 566–568.
68. Hall, L. & Rueckert, R.R. (1971). Infection of mouse fibroblasts by cardioviruses: premature uncoating and its prevention by elevated pH and magnesium chloride. *Virology* **43**, 152–165.
69. Bullough, P.A., Hughson, F.M., Skehel, J.J. & Wiley, D.C. (1994). Structure of influenza haemagglutinin at the pH of membrane fusion. *Nature* **371**, 37–43.
70. Muckelbauer, J.K., *et al.*, & Rossmann, M.G. (1995). The structure determination of coxsackievirus B3 to 3.5 Å resolution. *Acta Crystallogr. D.*, in press.
71. Rossmann, M.G. & Argos. P. (1976). Exploring structural homology of proteins. *J. Mol. Biol.* **105**, 75–95.
72. Liljas, L., Lindberg, M.A. & Pettersson, U. (1993). Modelling of the tertiary structure of CVB3 from the structure of poliovirus and rhinovirus. *Scand. J. Infect. Dis. Suppl.* **89**, 15–24.
73. Lindberg, M.A., Stålhandske, P.O.K. & Pettersson, U. (1987). Genome of coxsackievirus B3. *Virology* **156**, 50–63.
74. Gauntt, C.J., Trousdale, M.D., LaBadie, D.R.L., Paque, R.E. & Nealon, T. (1979). Properties of coxsackievirus B3 variants which are amyocarditic or myocarditic for mice. *J. Med. Virol.* **3**, 207–220.
75. Klump, W.M., Bergmann, I., Müller, B.C., Ameis, D. & Kandolf, R. (1990). Complete nucleotide sequence of infectious coxsackievirus B3 cDNA: two initial 5′ uridine residues are regained during plus-strand RNA syntheses. *J. Virol.* **64**, 1573–1583.
76. Tracy, S., Chapman, N.M. & Tu, Z. (1992). Coxsackievirus B3 from an infectious cDNA is cardiovirulent in mice. *Arch. Virol.* **122**, 398–409.
77. Chapman, N.M., Tu, Z., Tracy, S. & Gauntt, C.J. (1994). An infectious cDNA copy of the genome of a non-cardiovirulent coxsackievirus B3 strain: its complete sequence analysis and comparison to the genomes of cardiovirulent coxsackieviruses. *Arch. Virol.* **135**, 115–130.
78. Nicholls, A., Sharp, K. & Honig, B. (1991). Protein folding and association: insights from the interfacial and thermodynamic properties of hydrocarbons. *Proteins* **11**, 281–296.

Received: **28 Mar 1995**; revisions requested: **21 Apr 1995**; revisions received: **4 May 1995**. Accepted: **4 May 1995**.